



Jun Xie · Shuai Hao · Wenshuai Wang · Pengpeng Shi 

# Analytical solution of stress in functionally graded cylindrical/spherical pressure vessel

Received: 22 October 2020 / Accepted: 25 April 2021 / Published online: 19 May 2021  
© The Author(s), under exclusive licence to Springer-Verlag GmbH Germany, part of Springer Nature 2021

**Abstract** For the exact solution of the stress in the functionally graded (FG) cylindrical/spherical pressure vessel, this paper presents a unified form of the basic equations of the FG hollow cylinder/spherical shell by introducing parameter, and then, the axial/spherical symmetry mechanical problems of FG hollow shells are studied under three different boundary conditions, respectively. Assume that the Young's modulus of the material changes with thickness distribution of cylinder/shell in the form of power functions and the value of Poisson's ratio is constant, the analytical solutions of the displacement and stress of the FG hollow cylindrical/spherical pressure vessel are derived under different boundary conditions. By comparing the analytical solutions of the FG hollow cylinder/spherical shell obtained in this paper with the existing classical theoretical solutions and numerical solutions, the correctness of the analytical solution given in this paper is verified. In the numerical discussion, the distributions of displacement, radial stress and circumferential stress of the FG hollow cylinder/spherical shell under different gradient parameters and different size conditions are given, respectively. Finally, based on the difference numerical method, the stress distribution of FG hollow cylinder/spherical shell with the Young's modulus and Poisson's ratio along thickness distribution in the form of power functions is analyzed numerically. The results show that gradient parameter and geometric size have a great influence on the mechanical response of FG structure under different boundary conditions.

**Keywords** Functionally graded material (FGM) · Hollow cylinder/spherical shell · Stress distribution · Analytical solution · Axial/spherical symmetry problem

## 1 Introduction

Composite materials have great application in the engineering and the sudden change in the properties of most composite materials often cause obvious local stress concentration and material failure. The functionally graded material (FGM) [1, 2], as a special composite material, is generally composed of two or more materials, and its microstructure changes from one continuous and smooth material to another material with a specific gradient. So, the material properties of the FGM (including Young's modulus, shear modulus and material density) present a gradient change within a specific size range [3, 4]. As the development of traditional laminated materials, FGMs have many advantages, including reducing in-plane and lateral stress, reducing stress intensity

---

J. Xie · W. Wang (✉) · P. Shi (✉)  
School of Mathematics and Statistics, Ningxia University, Ningxia, Yinchuan 750021, China  
e-mail: wws@nxu.edu.cn

P. Shi  
e-mail: shipengpeng@xjtu.edu.cn

S. Hao · P. Shi  
School of Civil Engineering and Institute of Mechanics and Technology, Xi'an University of Architecture and Technology, Xi'an 710055, Shaanxi, China

factors, improving residual stress distribution and enhancing thermal performance [5]. Therefore, FGMs have been widely used in aerospace, mechanical engineering, biomedicine and other fields.

In order to obtain the analytical solution of the mechanical response of FGM structure, in theoretical research, it is often assumed that the Young's modulus changes with the spatial coordinates in the form of some special functions. Many researchers have studied the analytical solutions for FGM structures with changing material properties along the thickness direction. Pradhan and Chakraverty [6] studied the free vibration of functionally graded (FG) beams under different boundary conditions. Kang.

Kang and Li [7] analyzed the large deformation of the nonlinear cantilever FG beam and derived the explicit expressions of the deflection and rotation for FG beam subjected to end bending moment, and the influences of Young's modulus gradient distribution and material nonlinear parameters on the deflection of FG beam were analyzed. Li [8] extended the high-order theory to FG beams with continuously changing material properties and calculated numerically the FG cantilever beams with gradient index obeying the power law and showed graphically the effect of gradient index on deflection and stress distribution. By using the superposition principle method, Jiang and Ding [9] derived the analytic solution of the orthotropic FG cantilever beam. Ding et al. [10] considered the plane stress problem of a general anisotropic beam whose elastic compliance parameter was an arbitrary function of the thickness coordinate, and obtained the solutions for tension, pure bending beams, cantilever beam subjected to free end shear and cantilever beams or simply supported beams under uniform load.

In addition, FG hollow cylinders and spherical shells are commonly used in engineering. Some researchers have been carried out the research on FG vessel such as cylinders and spheres. For the FG cylindrical/spherical pressure vessel, it was assumed that the Young's modulus of the material changes with thickness distribution of cylinder/shell in the form of some special functions to solve the analytical solution of the problem in many papers. Horgan and Chan [11] proposed the linear elastic problem of FG hollow cylinder under internal pressure and studied the FG cylinder model under mechanical stress. Sarathchandra et al. [12] carried out modeling and structural analysis of FG cylindrical shells with different inner and outer surface compositions and carried out static structural analysis of cylindrical shells under internal pressure and then verified the analysis results with analytical solutions. Horgan and Chan [13] assumed that the Young's modulus changes with radial direction in the form of power functions and studied the one-dimensional axisymmetric deformation of a FG rotating disk. Li et al. [14] obtained the analytical solution of an isotropic FG ring under uniform load by introducing an appropriate logarithmic function term in the displacement expression when the inner and outer boundary conditions were in any combination. Tutuncu and Ozturk [1] studied FG spherical and cylindrical pressure vessels with the change of Young's modulus satisfying the power function along thickness distribution and gave the analytical solutions of stress. Tutuncu and Temel [15] obtained the stress and displacement equations of FG axisymmetric hollow spheres, cylinders and disks under uniform pressure. Ghannad et al. [16] studied the analytical solutions of the deformation and stress of axisymmetric thick cylindrical shells that were clamped along the edges and the FG with changing thickness was under internal pressure. Li et al. [17] proposed a new simple and effective integral equation method to study the FG axisymmetric structure with arbitrary gradient changes and solved the problem by transforming the considered problem into solving the integral equation. Chirag and Srikant [18] used the variation asymptotic method to obtain the asymptotically accurate analytical solution of the FG cylinder and analyzed the influence of the internal and external material properties, radius and material composition on the mechanical properties of the material. In addition, researchers also considered the influence of temperature load on the stress law of FG. Bahtui and Eslami [19] studied the thermoelastic coupling response of a FG cylindrical shell, and the thermoelastic coupling equation and energy equation of FG axisymmetric cylindrical shell under thermal shock load were solved. Subsequently, Bahtui and Eslami [20] studied the response of FG cylindrical thin shells based on the generalized thermoelastic theory. Assuming that the volume fraction of metal and ceramics is power law distribution, the influence of the temperature field on the linear and nonlinear distribution of shell thickness was studied. Jabbari et al. [21] studied the accurate solutions of the steady two-dimensional axisymmetric mechanical and thermal stresses on FG hollow cylinder.

This paper presents a unified form of the basic equations of the FG hollow cylinder/spherical shell by introducing parameter  $\delta$  and further discusses the stress distribution of the FG cylindrical/spherical pressure vessel under different boundary conditions. Assuming that Young's modulus of the material changes with radial direction in the form of power functions and the value of Poisson's ratio is constant, a derivation scheme is proposed to obtain the pressure distribution of the FG hollow cylinder/spherical shell under three different boundary conditions, respectively. Then, the analytical solution of stress distribution of FG hollow cylinder/spherical pressure vessel is compared with the numerical solution and the classical solution. Some analytical solutions in Ref [1] are corrected, which confirms the correctness of the results in this paper. In

addition, the stress distribution of FG hollow cylinder/spherical shell with the change of Poisson's ratio is numerically analyzed. Finally, some remarks and conclusions are given.

## 2 Basic equations and boundary conditions

### 2.1 basic equation

Considering the stress distribution of the FG cylindrical/spherical pressure vessel, the radial coordinate  $\bar{r}$  and displacement  $\bar{u}$  are normalized:  $r = \bar{r}/R$  and  $u = \bar{u}/R$ , where  $R$  is the outer radius of the cylindrical/spherical shell. It is assumed that the material is isotropic with constant Poisson's ratio and radially varying Young's modulus is approximated by  $E(r) = E_0 r^\beta$ , where  $E_0$  is the Young's modulus of the inner surface and  $\beta$  is the gradient constant.

The unified geometric equations of the cylindrical/spherical pressure vessel are established as following

$$\begin{aligned}\varepsilon_r &= \frac{du}{dr}, & \varepsilon_\theta &= \varepsilon_\phi = \frac{u}{r} \\ \gamma_{r\theta} &= \gamma_{r\phi} = \gamma_{\theta\phi} = 0\end{aligned}\quad (1)$$

Constitutive equations are

$$\begin{aligned}\sigma_r &= C_{11}\varepsilon_r + (\delta + 1)C_{12}\varepsilon_\theta \\ \sigma_\theta &= C_{12}\varepsilon_r + C_{11}\varepsilon_\theta + \delta C_{12}\varepsilon_\phi\end{aligned}\quad (2)$$

where  $\delta$  is parameter, and

$$\begin{aligned}C_{11} &= c_{11}r^\beta = \frac{E_0(1-\nu)}{(1+\nu)(1-2\nu)}r^\beta \\ C_{12} &= c_{12}r^\beta = \frac{E_0\nu}{(1+\nu)(1-2\nu)}r^\beta\end{aligned}\quad (3)$$

Equilibrium equation is

$$\frac{d\sigma_r}{dr} + \frac{(\delta + 1)(\sigma_r - \sigma_\theta)}{r} = 0\quad (4)$$

Here, this paper presents a unified form of the basic equations of the FG hollow cylinder/spherical shell by introducing parameter  $\delta$ . It can be seen that when the parameter  $\delta$  is 0, the basic equation given here can degenerate to get the basic equation of the axisymmetric problem for the FG cylindrical pressure vessel. When the parameter  $\delta$  is 1, the basic equation given here can degenerate to get the basic equation of the spherical symmetry problem for the FG spherical shell pressure vessel. The basic equations of the two kinds pressure vessels obtained by degradation are consistent with the basic equations given in Ref [1]. However, when  $\delta$  is chosen as a value between 0 and 1, the corresponding real physical problem has not been found yet at present. Here the parameter  $\delta$  realizes the unification of the basic equations of thick-walled cylindrical and spherical shell pressure vessels. This paper can realize the solutions of FG hollow cylindrical/spherical pressure vessels based on the basic equations in a unified form.

## 3 Boundary conditions

Considering the radial polarization of FG hollow cylinder/spherical shell, the inner and outer diameters are  $a$  and  $R$ , respectively, so the thickness of the hollow cylinder/spherical shell is  $R-a$ . Here, three different boundary conditions are considered here. Respectively, the inner surface is under pressure  $P$  and the outer surface is under tension  $Q$ (Case A); the inner boundary displacement is 0 and the outer boundary is under tension  $Q$ (Case B); and the inner boundary is under pressure  $P$  and the outer boundary displacement is 0(Case C). The boundary conditions are expressed as following.

Case A

$$\sigma_r(a/R) = -P, \sigma_r(1) = \sigma_r(R/R) = Q\quad (5)$$

Case B

$$u(a/R) = 0, \sigma_r(1) = \sigma_r(R/R) = Q \quad (6)$$

Case C

$$\sigma_r(a/R) = -P, u(1) = u(R/R) = 0 \quad (7)$$

## 4 Problem solving

### 4.1 Analytical solution of displacement

Using Eqs. (1)–(3), the governing equation of radial displacement becomes

$$r^2 u'' + (\beta + (\delta + 1))ru' + (v^* \beta - 1)(\delta + 1)u = 0 \quad (8)$$

where  $v^* = v/(1 - v)$ . Equation (8) is the Euler–Cauchy equation, and the characteristic equation is

$$m^2 + (\beta + \delta)m + (v^* \beta - 1)(\delta + 1) = 0 \quad (9)$$

Its root is

$$\begin{cases} m_1 = \frac{1}{2} \left( -\beta - \delta - \sqrt{(\beta + \delta)^2 - 4(v^* \beta - 1)(\delta + 1)} \right) \\ m_2 = \frac{1}{2} \left( -\beta - \delta + \sqrt{(\beta + \delta)^2 - 4(v^* \beta - 1)(\delta + 1)} \right) \end{cases} \quad (10)$$

These roots may be: (a) different real roots, (b) double roots and (c) complex conjugate roots. For different real roots, the solution of Eq. (8) is

$$u = Ar^{m_1} + Br^{m_2} \quad (11)$$

For double roots  $m_1 = m_2 = m$ , the solution of Eq. (8) becomes

$$u = (A + B \ln r)r^m \quad (12)$$

In the case of complex roots  $m_1 = x + iy$ ,  $m_2 = x - iy$ , the solution of Eq. (8) is

$$u = [A \cos(y \ln r) + B \sin(y \ln r)]r^x \quad (13)$$

where  $A$  and  $B$  are unknown parameters that have nothing to do with  $r$ ,  $A$  and  $B$  can be calculated by boundary conditions.

Here, Eq. (9) has been proved rigorously to have two different real roots. The detailed process is shown in “Appendix” A. Therefore, the displacement expression uses Eq. (11). Next, for three different boundary conditions, the stress was solved in this paper.

For Case A, using Eq. (5), the constants  $A$  and  $B$  are

$$\begin{aligned} A &= -\frac{(P + Q(a/R)^\beta (a/R)^{m_2-1})(a/R)^{1-\beta}(1+v)(1-2v)}{((a/R)^{m_1} - (a/R)^{m_2})E_0(m_1(1-v) + (\delta + 1)v)} \\ B &= \frac{(Q(a/R)^{m_1-1}(a/R)^\beta + P)(a/R)^{1-\beta}(1+v)(1-2v)}{((a/R)^{m_1} - (a/R)^{m_2})E_0(m_2(1-v) + (\delta + 1)v)} \end{aligned} \quad (14)$$

For Case B, using Eq. (6), the constants  $A$  and  $B$  are

$$\begin{aligned} A &= -\frac{Q(a/R)^{m_2}}{(a/R)^{m_1} \frac{m_2 E_0(1-v) + (\delta + 1)E_0 v}{(1+v)(1-2v)} - (a/R)^{m_2} \frac{m_1 E_0(1-v) + (\delta + 1)E_0 v}{(1+v)(1-2v)}} \\ B &= \frac{Q(a/R)^{m_1}}{(a/R)^{m_1} \frac{m_2 E_0(1-v) + (\delta + 1)E_0 v}{(1+v)(1-2v)} - (a/R)^{m_2} \frac{m_1 E_0(1-v) + (\delta + 1)E_0 v}{(1+v)(1-2v)}} \end{aligned} \quad (15)$$

For Case C, using Eq. (7), the constants  $A$  and  $B$  are

$$A = -\frac{P(a/R)^{-\beta}}{(a/R)^{m_1-1} \frac{m_1 E_0(1-v)+(\delta+1)E_0 v}{(1+v)(1-2v)} - (a/R)^{m_2-1} \frac{m_2 E_0(1-v)+(\delta+1)E_0 v}{(1+v)(1-2v)}} \quad (16)$$

$$B = \frac{P(a/R)^{-\beta}}{(a/R)^{m_1-1} \frac{m_1 E_0(1-v)+(\delta+1)E_0 v}{(1+v)(1-2v)} - (a/R)^{m_2-1} \frac{m_2 E_0(1-v)+(\delta+1)E_0 v}{(1+v)(1-2v)}}$$

The displacement solutions of the FG hollow cylinder/spherical shell can be directly obtained by Eq. (11).

#### 4.2 Stress analytical solution

Further combining Eqs. (1) and (2), the radial stress and circumferential stress of the FG hollow cylinder/spherical shell can be finally obtained. The corresponding stress analytical solutions in Case A are

$$\sigma_r = r^{\beta-1} \left(\frac{a}{R}\right)^{1-\beta} \frac{(P + Q(a/R)^{m_1-1}(a/R)^\beta)r^{m_2} - (P + Q(a/R)^\beta(a/R)^{m_2-1})r^{m_1}}{(a/R)^{m_1} - (a/R)^{m_2}} \quad (17)$$

$$\sigma_\theta = \frac{(a/R)^{1-\beta} r^{\beta-1} (\chi_1 - \chi_2)}{[m_1(v-1) - (\delta+1)v][m_2(v-1) - (\delta+1)v]((a/R)^{m_1} - (a/R)^{m_2})}$$

where

$$\begin{cases} \chi_1 = (P + Q(a/R)^\beta(a/R)^{m_1-1})r^{m_2}(vm_2 + (1-v) + \delta v)[m_1(1-v) + (\delta+1)v] \\ \chi_2 = (P + Q(a/R)^\beta(a/R)^{m_2-1})r^{m_1}(vm_1 + (1-v) + \delta v)[m_2(1-v) + (\delta+1)v] \end{cases} \quad (18)$$

The corresponding stress analytical solutions in Case B are

$$\sigma_r = \frac{Qr^\beta((a/R)^{m_1}r^{m_2-1}(m_2(1-v) + (\delta+1)v) - (a/R)^{m_2}r^{m_1-1}(m_1(1-v) + (\delta+1)v))}{(a/R)^{m_1}(m_2(1-v) + (\delta+1)v) - (a/R)^{m_2}(m_1(1-v) + (\delta+1)v)} \quad (19)$$

$$\sigma_\theta = \frac{Qr^\beta((a/R)^{m_1}r^{m_2-1}((1-v) + m_2v + \delta v) - (a/R)^{m_2}r^{m_1-1}(m_1v + (1-v) + \delta v))}{(a/R)^{m_1}(m_2(1-v) + (\delta+1)v) - (a/R)^{m_2}(m_1(1-v) + (\delta+1)v)}$$

The corresponding stress analytical solutions in Case C are

$$\sigma_r = \frac{Pr^\beta((1-v)(m_2r^{m_2-1} - m_1r^{m_1-1}) + (\delta+1)v(r^{m_2-1} - r^{m_1-1}))}{\left(\frac{a}{R}\right)^{\beta+m_1-1}(m_1(1-v) + (\delta+1)v) - \left(\frac{a}{R}\right)^{\beta+m_2-1}(m_2(1-v) + (\delta+1)v)} \quad (20)$$

$$\sigma_\theta = \frac{Pr^\beta((1-v)(r^{m_2-1} - r^{m_1-1}) + v(m_2r^{m_2-1} - m_1r^{m_1-1}) + \delta v(r^{m_2-1} - r^{m_1-1}))}{\left(\frac{a}{R}\right)^{\beta+m_1-1}(m_1(1-v) + (\delta+1)v) - \left(\frac{a}{R}\right)^{\beta+m_2-1}(m_2(1-v) + (\delta+1)v)}$$

When the parameter  $\delta$  is 0, the stress distributions Eqs. (17)–(20) can degenerate to obtain the stress distribution of the FG cylinder under three different boundary conditions. The detailed expression is shown in “Appendix” B. When the parameter  $\delta$  is 1, the stress distribution Eqs. (17)–(20) can degenerate to obtain the stress distribution of the FG spherical shell under three different boundary conditions. The detailed expression is shown in “Appendix” C.

## 5 Result verification and analysis

### 5.1 Comparative verification

Now, considering the FG cylindrical/spherical pressure vessel is only subjected to internal pressure, that is  $Q = 0$  in Case A, the radial stress and circumferential stress of the hollow cylinder are, respectively,

$$\begin{aligned}\sigma_r &= r^{\beta-1}(a/R)^{1-\beta} \frac{P(r^{m_2} - r^{m_1})}{(a/R)^{m_1} - (a/R)^{m_2}} \\ \sigma_\theta &= \frac{(a/R)^{1-\beta} r^{\beta-1} (\chi_1 - \chi_2)}{[m_1(v-1) - v][m_2(v-1) - v]((a/R)^{m_1} - (a/R)^{m_2})}\end{aligned}\quad (21)$$

where

$$\chi_1 = Pr^{m_2}(vm_2 + (1-v))[m_1(1-v) + v]\chi_2 = Pr^{m_1}(vm_1 + (1-v))[m_2(1-v) + v].$$

The radial stress and circumferential stress of the spherical shell are, respectively,

$$\begin{aligned}\sigma_r &= r^{\beta-1}(a/R)^{1-\beta} \frac{P(r^{m_2} - r^{m_1})}{(a/R)^{m_1} - (a/R)^{m_2}} \\ \sigma_\theta &= \frac{(a/R)^{1-\beta} r^{\beta-1} (\chi_1 - \chi_2)}{[m_1(v-1) - 2v][m_2(v-1) - 2v]((a/R)^{m_1} - (a/R)^{m_2})}\end{aligned}\quad (22)$$

where

$$\chi_1 = Pr^{m_2}(vm_2 + 1)[m_1(1-v) + 2v]\chi_2 = Pr^{m_1}(vm_1 + 1)[m_2(1-v) + 2v].$$

However, the radial stress and circumferential stress of the FG cylindrical vessel under internal pressure in Ref [1] are, respectively,

$$\begin{aligned}\sigma_r &= -P(a/R)^{1-\beta} \frac{(r^{m_1} - r^{m_2})r^{\beta-1}}{(a/R)^{m_1} - (a/R)^{m_2}} \\ \sigma_\theta &= \frac{P(a/R)^{1-\beta} (\chi_1 - \chi_2)}{((a/R)^{m_1} - (a/R)^{m_2})[(v-1)m_1 - v][m_2(v-1) - v]}\end{aligned}\quad (23)$$

where

$$\begin{cases} m_1 = 0.5 \left( -\beta - \sqrt{4 + \beta^2 - 4v^*\beta} \right) \\ m_2 = 0.5 \left( -\beta + \sqrt{4 + \beta^2 - 4v^*\beta} \right) \\ \chi_1 = r^{m_1} (m_2(v-1) - v) [1 + (m_1 - 1)v] \\ \chi_2 = r^{m_2} (m_1(v-1) - v) [1 + (m_2 - 1)v] \end{cases}\quad (24)$$

The corresponding radial stress and circumferential stress of the FG spherical vessel under internal pressure in Ref [1] are

$$\begin{aligned}\sigma_r &= -P(a/R)^{1-\beta} \frac{(r^{m_1} - r^{m_2})r^{\beta-1}}{(a/R)^{m_1} - (a/R)^{m_2}} \\ \sigma_\theta &= \frac{P(a/R)^{1-\beta} (\chi_1 - \chi_2)}{((a/R)^{m_1} - (a/R)^{m_2})[m_1(v-1) - 2v][m_2(v-1) - 2v]}\end{aligned}\quad (25)$$

where

$$\begin{cases} m_1 = 0.5 \left( -\beta - 1 - \sqrt{\beta^2 + (2 - 8v^*)\beta + 9} \right) \\ m_2 = 0.5 \left( -\beta - 1 + \sqrt{\beta^2 + (2 - 8v^*)\beta + 9} \right) \\ \chi_1 = r^{m_1-1} [(m_2(v-1) - 2v)(v + r^\beta(1+(m_1-1)v))] \\ \chi_2 = r^{m_2-1} [(m_1(v-1) - 2v)(v + r^\beta(1+(m_2-1)v))] \end{cases} \quad (26)$$

The stress distributions of the FG hollow cylinder/spherical shell obtained in this paper are consistent with the radial stress expressions of the FG cylinder/sphere given in Ref [1], but the circumferential stress expressions are different [23]. The correctness of our proposed analytical solutions is discussed here. When  $\beta = 0$ , analytical solution in this paper can degenerate to the analytical solution of pressure vessels with homogeneous material. The degradation analytical solutions in this paper are completely consistent with those of the classic literature [22]. It is worth noting that the degradation result of the cylinder pressure vessel in Ref [1] is  $\sigma_\theta = -P(a/R)^2(r^2 + 1)/[r((a/R)^2 - 1)]$ , which is inconsistent with the classic result of the homogeneous cylindrical pressure vessels  $\sigma_\theta = -P(a/R)^2(r^2 + 1)/[r^2((a/R)^2 - 1)]$  in the classic literature [22]. This confirms some errors in the analytical solutions in Ref [1]. In addition, the finite element methods (FEM) are performed here. The comparison of our proposed analytical solution, FEM numerical solution and previous analytical solution in Ref [1] is given.

Figure 1 shows the comparison results of the radial and circumferential stresses of the FG hollow cylinder/spherical shell, that is, the results of this paper are compared with the results of Ref [1] and the numerical results. It can be seen from the figure that radial stress of the cylindrical/spherical pressure vessel in this paper is completely consistent with the radial stress given in Ref [1] and numerical results, and the circumferential stress calculated in this paper is completely consistent with the numerical results [23], but the results of circumferential stress in Ref [1] are completely different with the results in this paper and numerical results. As shown in Fig. 1a and b, the trend of radial stress distribution is the same for the FG cylinder/sphere in Case A. The absolute value of the radial stress decreases with increasing  $r$ , and the absolute value of the radial stress increases with increasing  $\beta$ . Figure 1c and d shows the circumferential stress distribution of FG cylindrical/spherical shell when  $\beta = [-2, 2]$ . From Fig. 1c and d, when  $\beta < 0$ , the circumferential stress of the hollow cylinder/spherical shell stress container gradually decreases with the increase of  $r$ . When  $\beta > 0$ , the circumferential stress increase with the increase of  $r$ . However, the result of Ref [1] is different. Regardless of the value selection of  $\beta$ , the circumferential stress shows a decreasing trend with the increase of  $r$ , which is quite different from the results of this paper and the numerical results. Figure 1 shows that the radial stress of the FG cylindrical/spherical pressure vessel is much smaller than the circumferential stress, so the failure of this vessel under internal pressure load is often caused by excessive circumferential stress. When  $\beta = -2$ , the circumferential stress reaches the maximum on the inner surface, and the maximum circumferential stress on the inner surface decreases with the increase of  $\beta$ . When the  $\beta$  exceeds a certain value, the circumferential stress is relatively evenly distributed inside the cylindrical/spherical shell. This feature is helpful for engineers to select a suitable gradient in the design of FG pressure vessels to reduce circumferential stress change in the structure and this feature can help to avoid cracking due to excessive circumferential stress.

## 5.2 The influence of different boundary conditions and structure types on dimensionless displacement distribution

Note that the  $u_0$  is displacement for homogeneous material under three boundary conditions. Here,  $u_0$  is used as a reference value for normalization. The expressions can also easily be obtained by setting  $\beta = 0$  in Eq. (10) and Eq. (11). In addition, the  $\sigma_r^0$  and  $\sigma_\theta^0$  are radial and circumferential stress for homogeneous material under three boundary conditions, respectively. The expressions are shown in "Appendix" D. The  $u_0$ ,  $\sigma_r^0$  and  $\sigma_\theta^0$  are studied by some researchers, such as the classic literature [22]. Figures 2 and 3 show the radial dimensionless displacement distribution of the FG cylindrical/spherical container under three different boundary conditions. As shown in Figs. 2a and 3a, the dimensionless displacement distribution of the FG cylinder/spherical shell increases with the increase of the gradient parameter  $\beta$ ; the dimensionless displacement hardly increases with the increase of  $r$  in Case A. For case B, since the boundary condition is internally fixed, as shown in Figs.

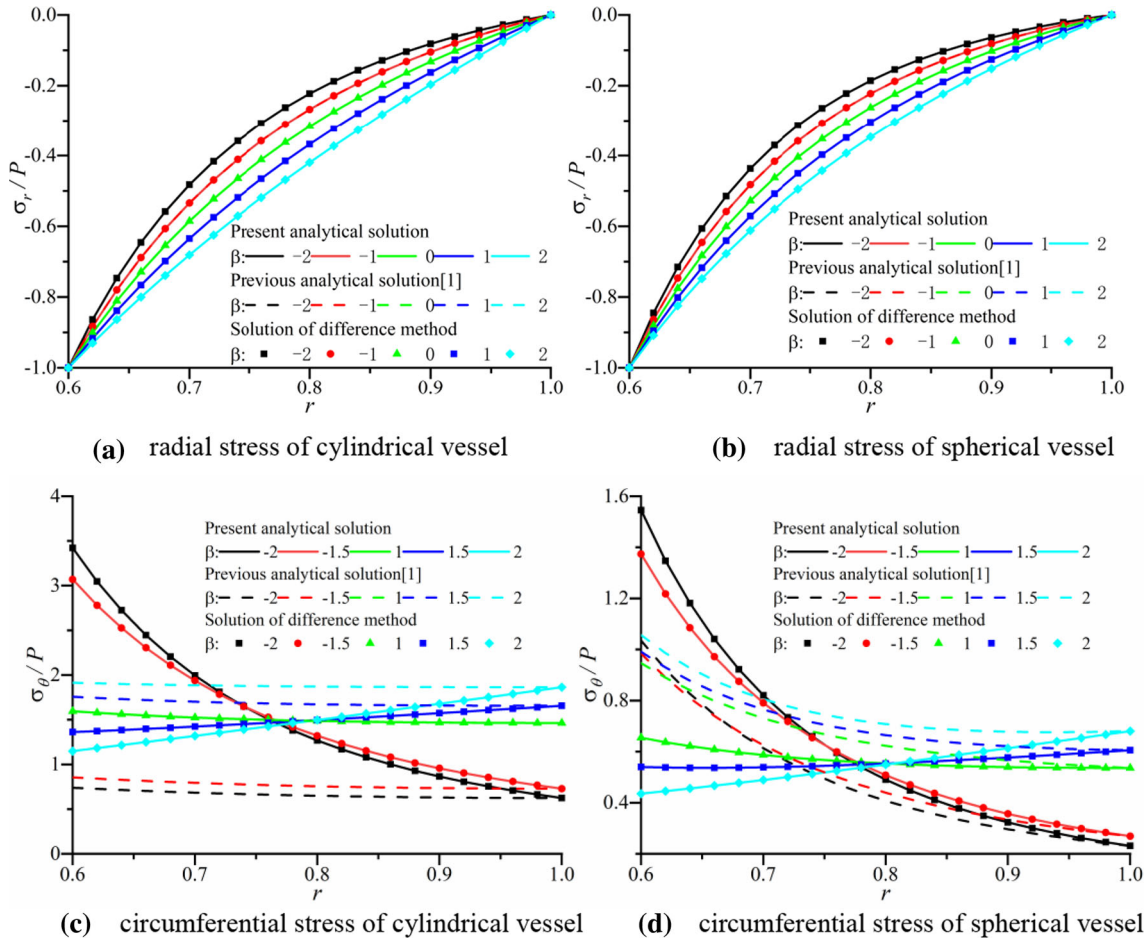


**Fig. 1** Stress distributions along the thickness direction of FG hollow cylindrical/spherical vessel under degraded boundary in Case A

2b and 3b, when  $\beta > 0$ , the dimensionless displacement decreases with the increase of  $r$ . When  $\beta < 0$ , the dimensionless displacement increases as  $r$  increases. As shown in Figs. 2c and 3c, under the boundary conditions of Case C, the dimensionless displacement distribution of the FG cylinder/spherical shell increases with the increase of the gradient parameter  $\beta$ . When  $\beta < 0$ , the dimensionless displacement increases with the increase of  $r$ ; when  $\beta > 0$ , the dimensionless displacement decreases with the increase of  $r$ .

5.3 The influence of different boundary conditions on stress distribution

Figures 4 and 5 show the radial and circumferential stress distributions of FG cylindrical/spherical vessels under three different boundary conditions. From Figs. 4a, b and 5a and b, it can be seen that under the boundary conditions of Case A, the radial stress of the FG cylindrical/spherical shell decreases with the increase of the gradient parameter  $\beta$ . When  $\beta > 0$ , the circumferential stress increases with the increase of  $r$ . When  $\beta < 0$ , circumferential stress decreases with the increase of  $r$ . The circumferential stress is higher than the radial stress. That is, the circumferential stress is very sensitive to the gradient parameter  $\beta$ , which also shows that the failure of cylindrical/spherical pressure vessel is often caused by excessive circumferential stress. For Case B, as shown in Figs. 4c, d and 5c and d, the radial stress of the FG hollow cylinder/spherical shell decreases with the increase of  $\beta$ . When the gradient parameter  $\beta > 0$ , the circumferential stress increases with the increase of  $r$ . When  $\beta < 0$ , the circumferential stress first increases with the increase of  $r$ , and then the increase tends to be flat nearby the dimensionless position  $r = 0.74$ . From Figs. 4e, f and 5e and f, it can be seen that under the boundary conditions of Case C, the radial stress distribution of the FG cylindrical/spherical shell increases with the increase of  $\beta$ . However, the absolute value of the circumferential stress distribution decreases with



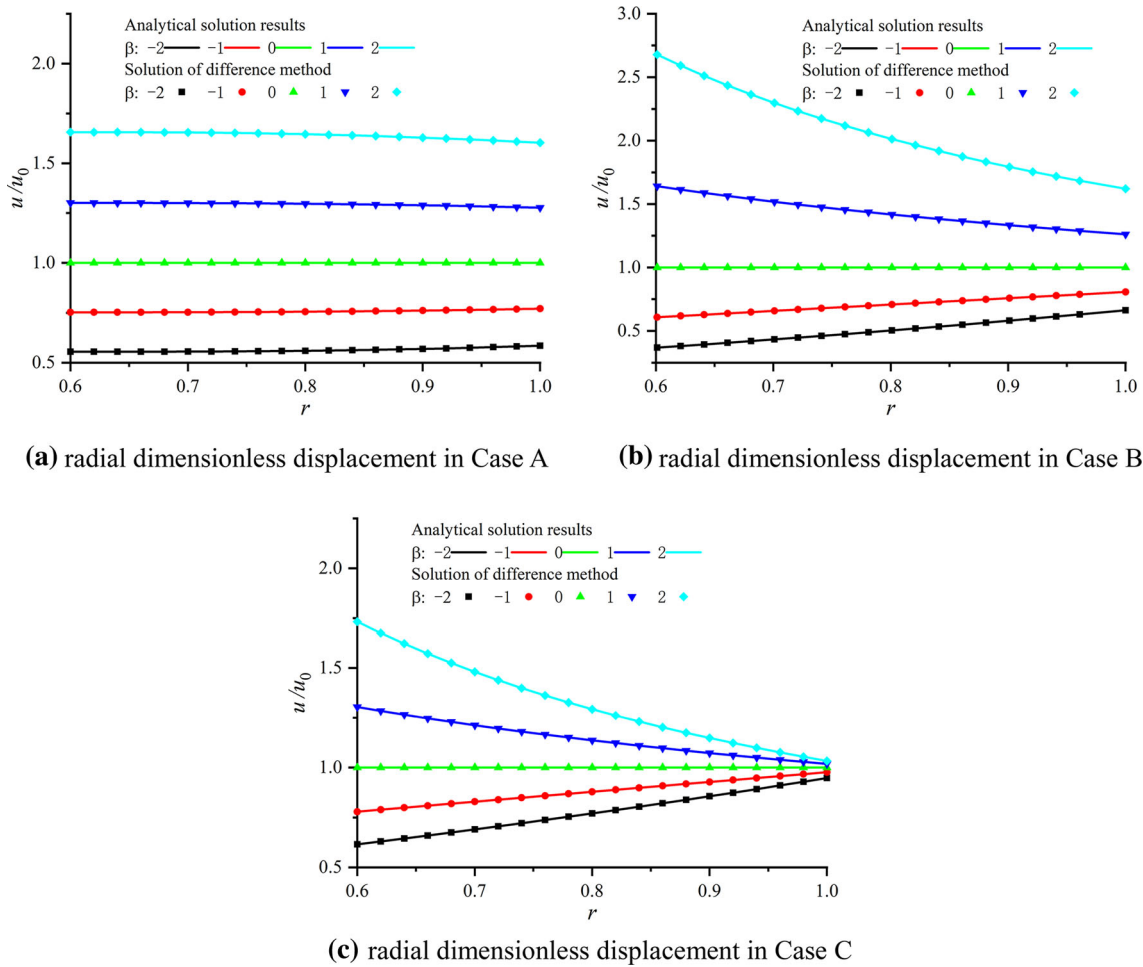


Fig. 2 Radial dimensionless displacement distribution of FG cylindrical vessel in three different boundary conditions

the increase of  $\beta$ , and the absolute value of the circumferential stress decreases with the increase of  $r$  and finally stabilizes. As shown in Figs. 4 and 5, the magnitude and sign of the gradient parameter  $\beta$  have a great influence on the circumferential stress under the three boundary conditions. It not only affects the absolute value of circumferential stress, but also affects the change trend of circumferential stress. This shows that the selection of appropriate gradient parameters can make the FG cylinder/spherical shell obtain the optimal stress distribution. Figures 4a, 5a, b, b, c, d and d show the absolute value of the radial and circumferential stress distribution of corresponding FG hollow cylindrical/spherical vessel under the same boundary conditions. It can be seen from Figs. 4 and 5 that under the same boundary conditions, the stress distribution trend of the FG cylindrical/spherical pressure vessel is consistent, which is easy to understand. However, the absolute value of the stress is different, which is determined by their geometric characteristics.

#### 5.4 The influence of geometric features (thickness) on stress distribution

Figures 6 and 8 show the influence of different dimensionless size  $r$  (cylindrical/spherical shell thickness) on the radial and circumferential stress distribution of the FG hollow cylindrical/spherical pressure vessel under different boundary conditions. Here the gradient parameter  $\beta$  is  $-2$ , the dimensionless size  $r$  is 0.2, 0.4 and 0.6, respectively. It can be seen from the figure that different thicknesses, that is the value selection of  $r$ , have no effect on change trend of the radial and circumferential stress for the cylindrical/spherical shell, but the value selection of  $r$  has a significant influence on the absolute value of the stress distribution in the FG cylindrical/spherical shell. It can be seen from in Figs. 6, 7 and 8 that under different thicknesses, the absolute value of the stress has a local maximum, and the magnitude of the extreme value is related to the value of

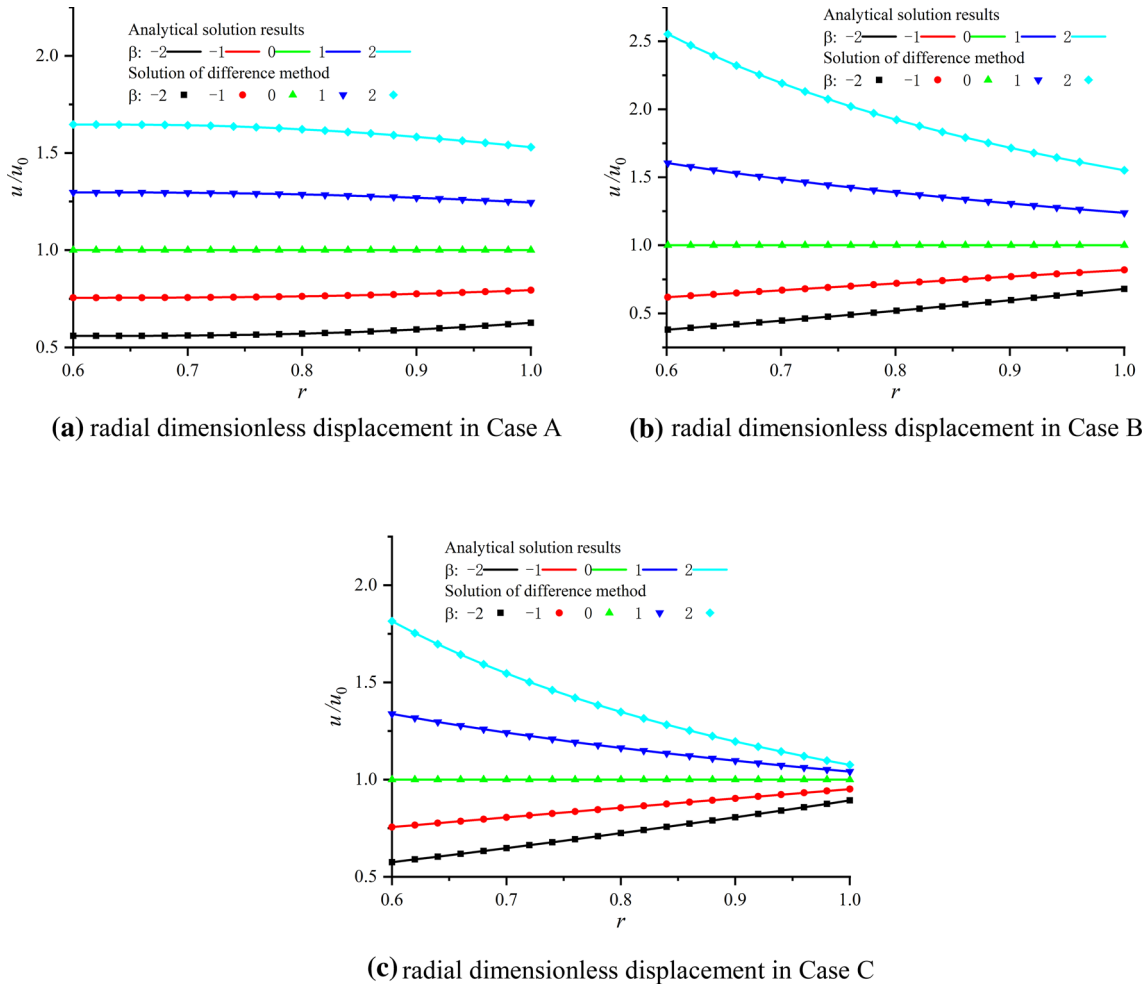


Fig. 3 Radial dimensionless displacement distribution of FG spherical shell vessel in three different boundary conditions

$r$ . Therefore, the thickness has a great influence on the radial and circumferential stress distribution of the FG cylindrical/spherical pressure vessel, which indicates that adjusting different sizes based on appropriate gradient parameters can achieve the optimal stress distribution for the FG cylindrical/spherical pressure vessel. Therefore, the most suitable material performance can be obtained, and device can be used more safely for people.

**6 The discussion on the FGMs with change both Young’s modulus and Poisson’s ratio**

In this subsection, it is assumed that the radially varying Young’s modulus and Poisson’s ratio are approximated by  $E(r) = E_0r^\beta$  and  $\nu(r) = \nu_0r^\alpha$ , where  $E_0$  and  $\nu_0$  are the Young’s modulus and Poisson’s ratio for the inner surface, respectively.  $\beta$  and  $\alpha$  are Young’s modulus and Poisson’s ratio gradient constant, respectively. The influence of the change of both Young’s modulus and Poisson’s ratio on the stress distribution is analyzed by numerical calculations. The numerical calculation process for this problem is shown in “Appendix” E.

FGMs were originally used to solve problems in the design and manufacture of thermal protection systems for the new generation of space shuttles. For the FGMs, on the relatively high temperature outer side is made of ceramics with excellent heat resistance, and the inner side is made of metal materials with high thermal conductivity, high toughness and high mechanical strength. The composition, microstructure and porosity of the composite material are adjusted to form the FG layer in the transition zone between on the inner and outer sides [2]. The application of FGMs avoids the interface stress caused by the huge difference between metals and ceramics in physical and mechanical properties. The Poisson’s ratio of ceramic materials and metal steel

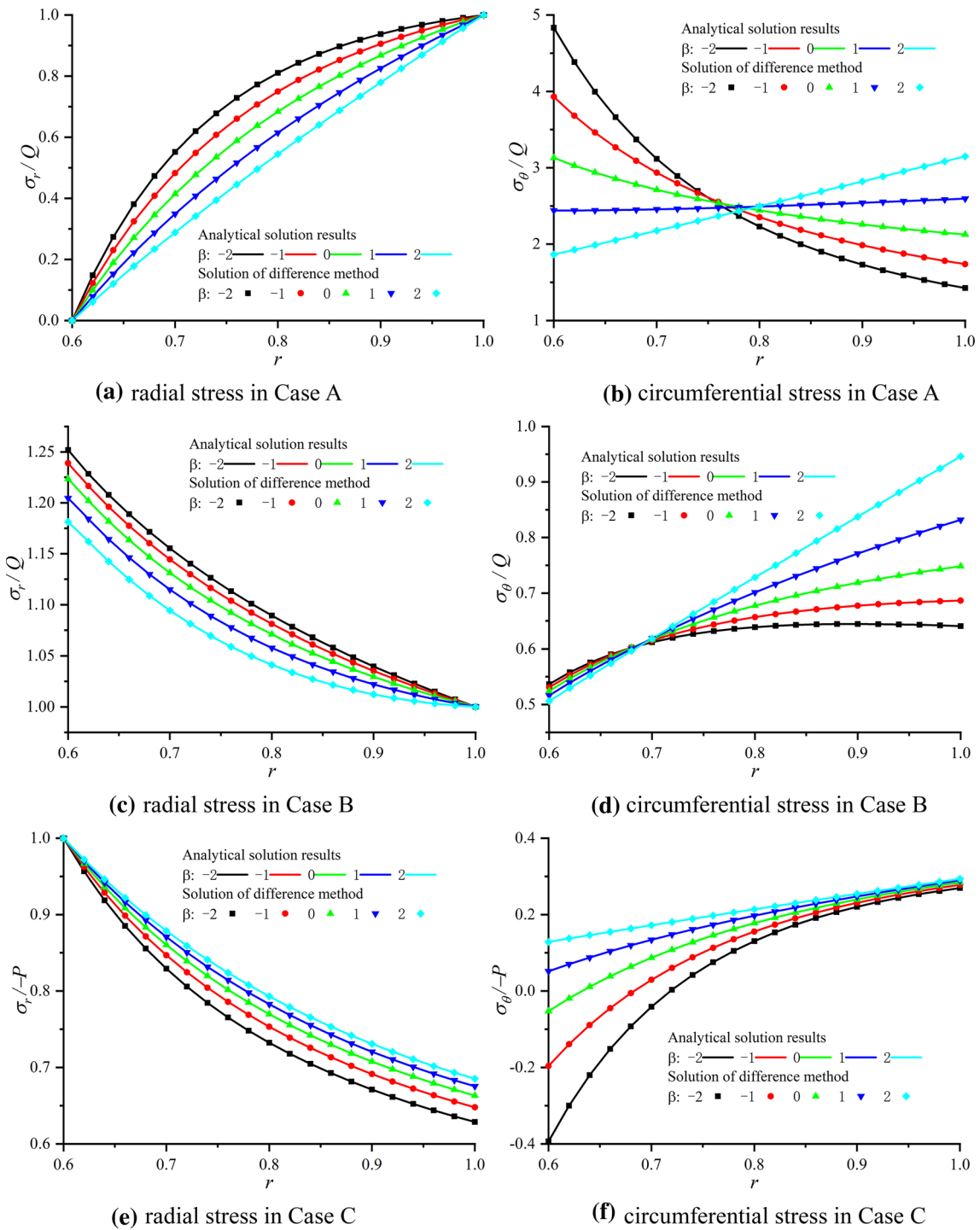


**Fig. 4** Stress distributions along the thickness direction of FG hollow cylindrical vessel (Solid lines: analytical solution of this paper, solid points: solution of finite difference method)

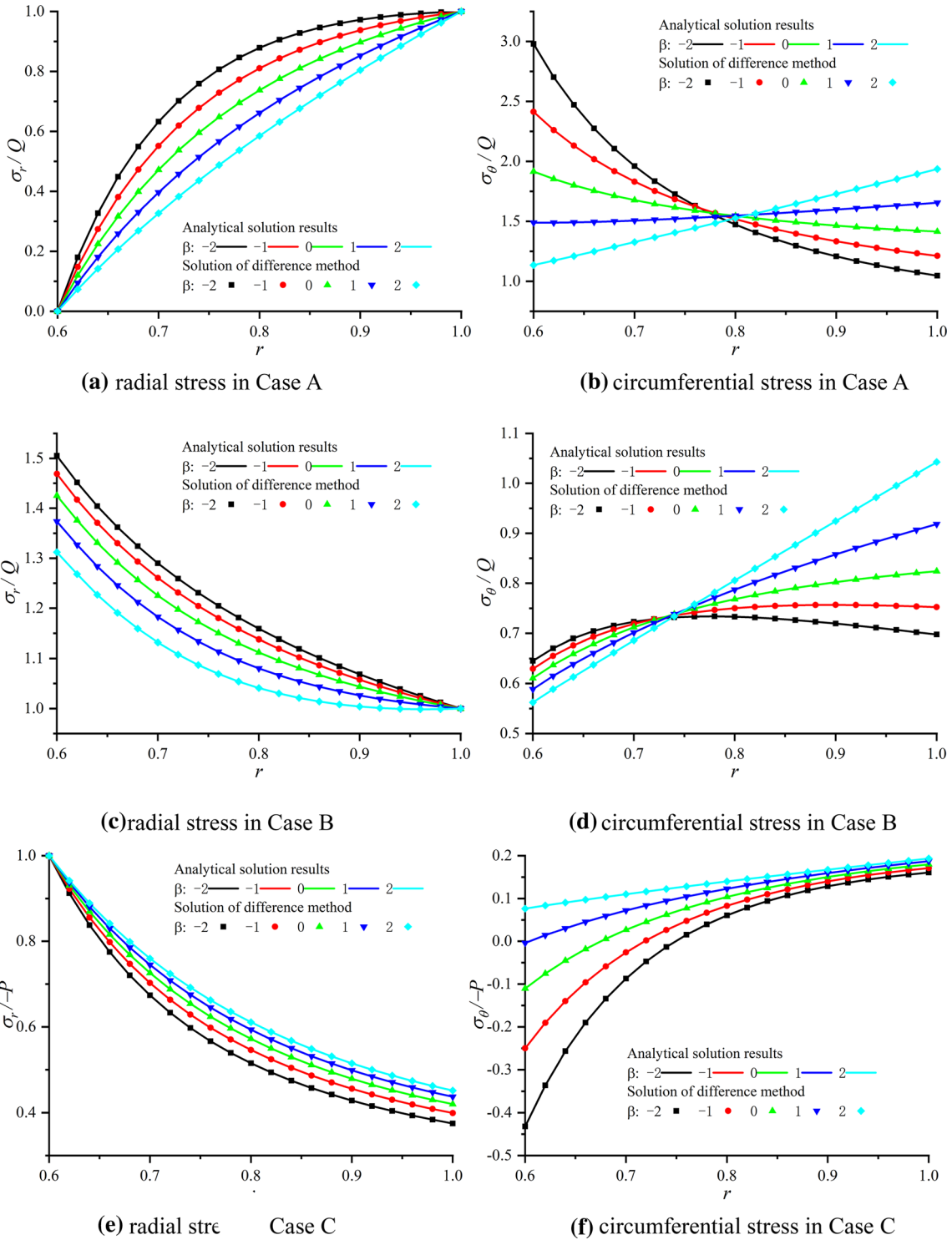


**Fig. 5** Stress distributions along the thickness direction of FG spherical vessel (Solid lines: analytical solution of this paper, solid points: solution of finite difference method)

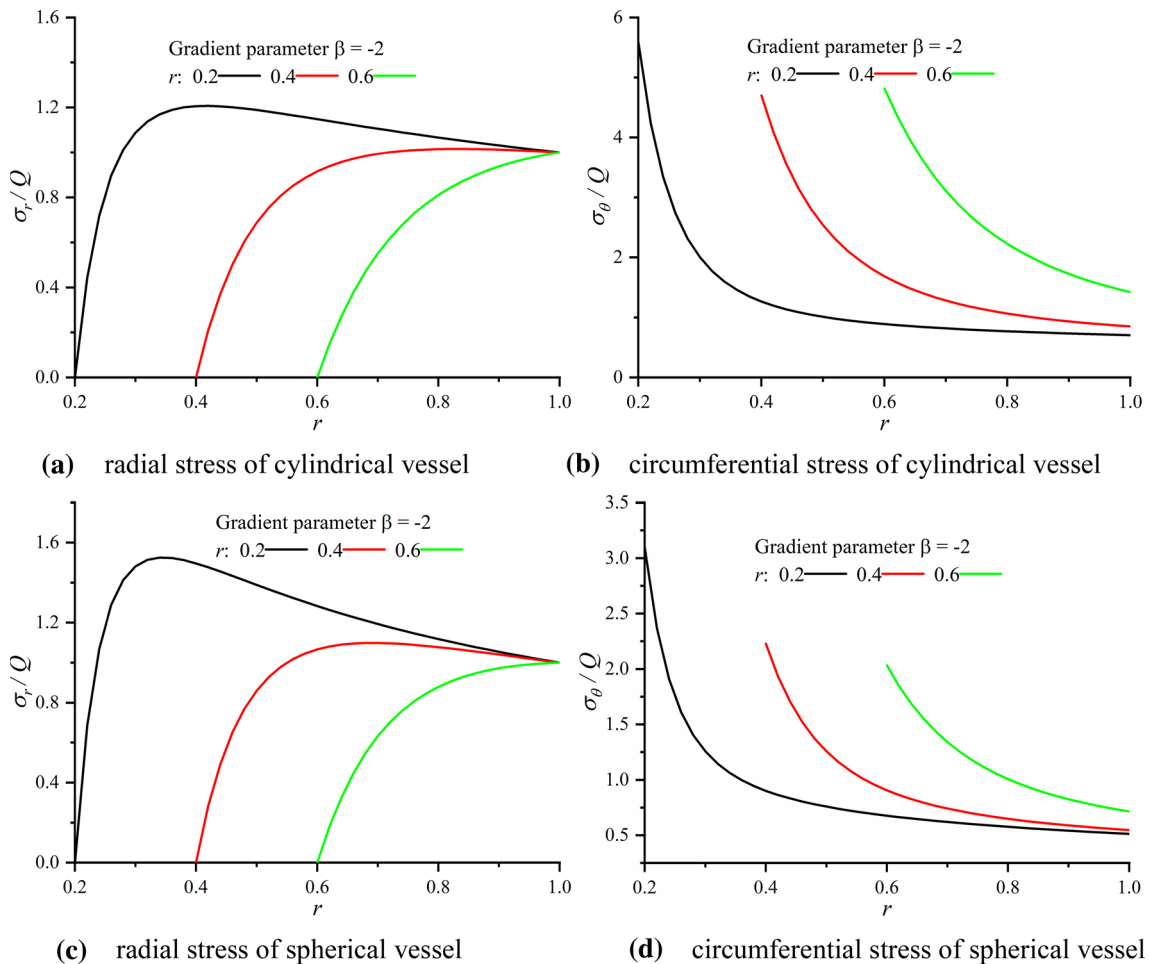


**Fig. 6** Different stress distributions of FG hollow cylinder/spherical shell in Case A

materials is 0.32 and 0.3, respectively. When the ratio of the inner radius for the hollow cylinder/spherical shell is  $a$ , one can obtain the Poisson's ratio gradient parameter  $\alpha = \log_a 0.32/0.3$ , where the Poisson's ratio of the inner metal material is 0.3 and the Poisson's ratio of the outer ceramic material is 0.32. Under this condition, the influence of Poisson's ratio on stress in FGMs is discussed numerically here. As shown in Fig. 9, in this condition, the Poisson's ratio gradient parameter has little effect on the stress distribution in Case A and Case C. But the change for Poisson's ratio has a greater effect on the stress distribution in Case B, especially for the radial stress. The radial and circumferential stresses of the FG hollow cylinder/spherical shell both decrease with the increase of the gradient parameter  $\alpha$  in Fig. 9c and d.

In addition, the influence of changes in Young's modulus and larger changes in Poisson's ratio on stress is considered. The gradient parameters are  $\beta = -2$ ,  $\alpha = -0.5, -0.2, 0, 0.2$  and  $0.5$ , respectively, in Fig. 10. It shows the influence of the change of Poisson's ratio on the stress. Figure 10a and b show that both the radial stress and the circumferential stress increase with the increase of  $\alpha$ . The change of Poisson's ratio has a greater effect on the circumferential stress for the FG cylinder and spherical shell. The circumferential stress of FG cylinder is approximately 1.5 times larger than that of spherical shell circumferential stress. As shown in Fig. 10c, f, the gradient parameter  $\alpha$  affects the change trend of the radial stress for FG hollow cylinder/spherical shell. When  $\alpha = -0.5$ , the radial stress increases with the increase of the  $\alpha$ , and when  $\alpha = -0.2, 0, 0.2$  and  $0.5$ , the radial stress decreases with the increase of  $\alpha$ , and some existing analytical solutions ignore the influence of the change of Poisson's ratio in the mechanical analysis of FGMs. Based on the difference numerical method, this paper confirms that the change of Poisson's ratio also has a greater effect on the stress distribution under certain conditions.

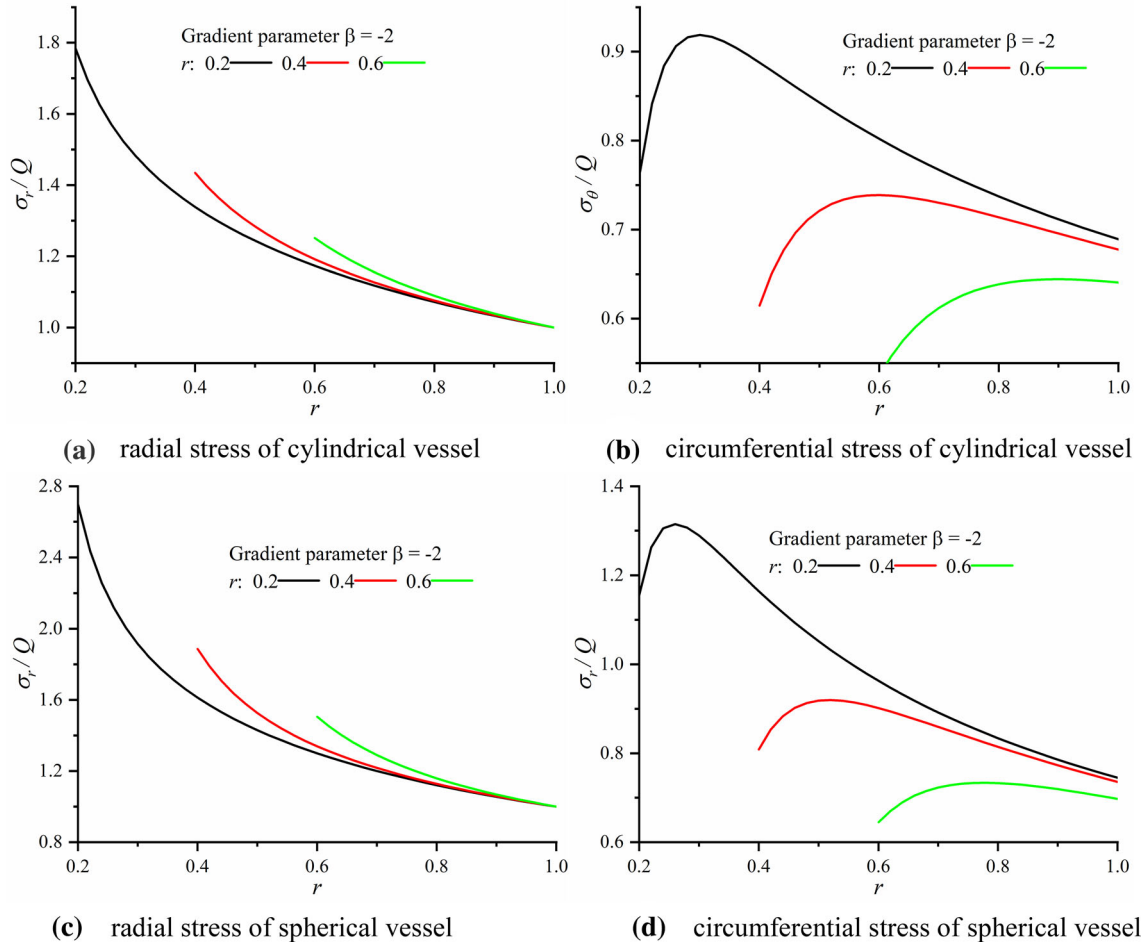
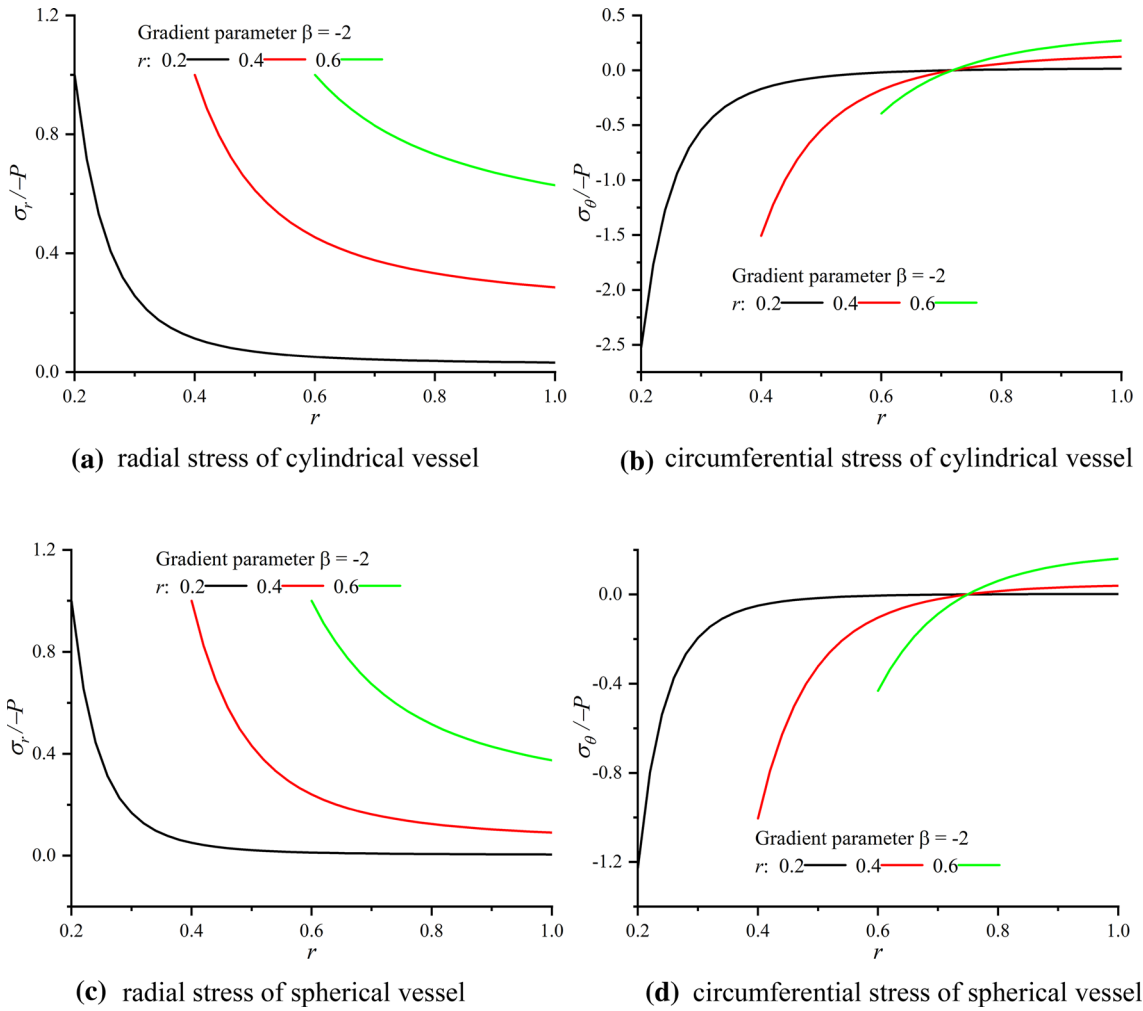


Fig. 7 Different stress distributions of FG hollow cylinder/spherical shell in Case B

### 7 Conclusion

This paper presents a unified form of the basic equations of the FG hollow cylinder/spherical shell by introducing parameter and studies the axial/spherical symmetry mechanical problems of the FG hollow cylinder/spherical shell under three different boundary conditions. Assuming that the value of Poisson’s ratio is constant and the Young’s modulus changes with radial direction in the form of power functions, the analytical solutions of the displacement, radial stress and the circumferential stress of the hollow cylindrical/spherical pressure vessel are given under three different boundary conditions. By comparison with the analytical solutions in the classical literature [22] and the numerical solutions by FEM, the errors of analytical solutions are corrected in Ref [1] when the inner surface is under pressure  $P$ . At the same time, by comparing with the results from the difference numerical method, the correctness of new analytical solutions for three different boundary conditions is confirmed in this paper. Analysis shows that the circumferential stress tends to be evenly distributed by adjusting the gradient parameter, which can effectively prevent container cracking caused by excessive circumferential stress, thereby improving the reliability and service life of the device. In addition, the influence of different geometric size (vessel thickness) on the stress distribution is analyzed. Finally, the influence of the change of Young’s modulus and Poisson’s ratio on stress is numerically discussed. Some existing analytical solutions ignore the influence of the change of Poisson’s ratio in the mechanical analysis of FGM. Based on the difference numerical method, this paper confirms that the change of Poisson’s ratio also has a significant effect on the stress distribution under certain conditions. Therefore, for the FG hollow cylindrical/spherical pressure vessel, selecting the appropriate gradient parameters and the appropriate thickness can make the FG pressure vessel achieve its optimal performance, which is helpful for engineering design. The method in this



**Fig. 8** Different stress distributions of FG hollow cylinder/spherical shell in Case C

paper is further promoted to be suitable for discussing the analysis of other FG piezoelectric and piezomagnetic materials [24].

**Acknowledgements** This work was supported by the National Natural Science Foundation of China [Grant No. 11802225].

**Appendix A**

Here, Eq. (9) has been proved rigorously to have two different real roots. The detailed process is as follows. When the parameter  $\delta$  is 0, Eq. (9) degenerates to

$$m^2 + \beta m + (v^* \beta - 1) = 0 \tag{A.1}$$

Most materials satisfy  $0 < v < 0.5$ . Because of  $v^* = v/(1 - v)$ ,  $v^*$  satisfies  $0 < v^* < 1$  and  $0 < v^{*2} < 1$ .

$$\Delta = \beta^2 - 4(v^* \beta - 1) = (\beta^2 - 2v^*)^2 + 4(1 - v^{*2}) > 0 \tag{A.2}$$

So Eq. (9) has two different real roots.

When the parameter  $\delta$  is 1, Eq. (9) degenerates to

$$m^2 + (\beta + 1)m + 2(v^* \beta - 1) = 0 \tag{A.3}$$

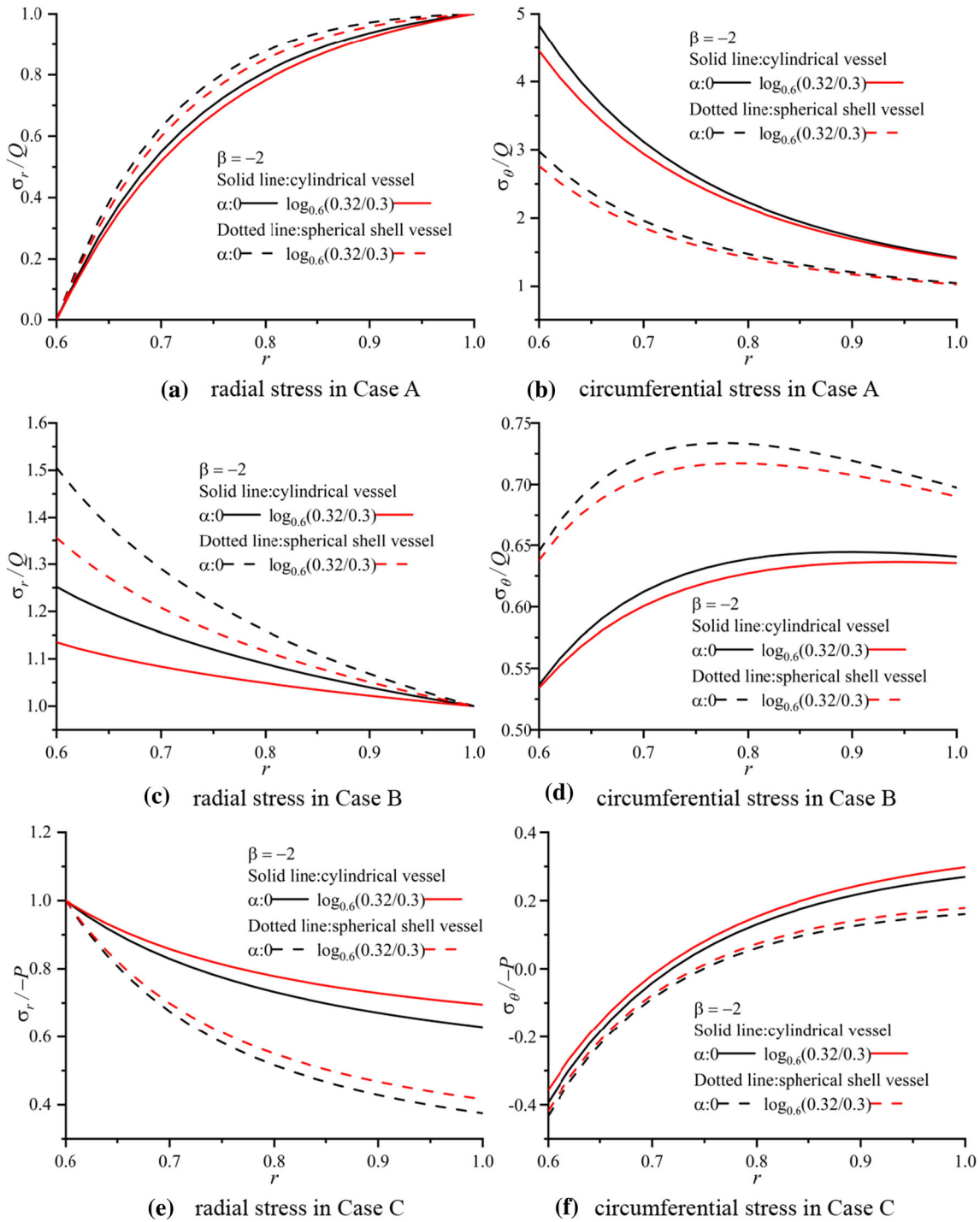


**Fig.9** Radial and circumferential stress distribution of FG cylinder/ spherical shell vessel



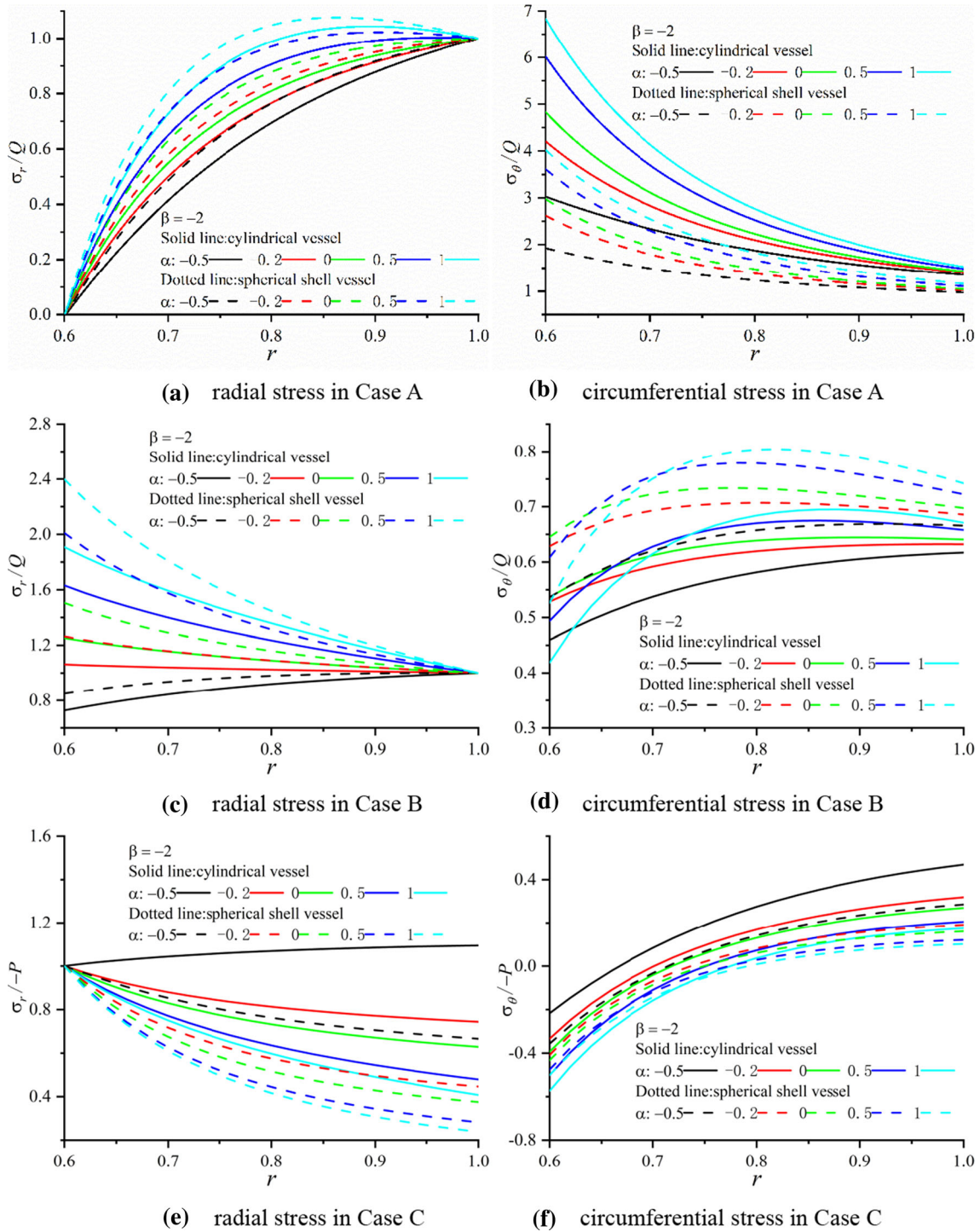


**Fig. 10** Radial and circumferential stress distribution of FG cylinder/spherical shell vessel

Since

$$\Delta = (\beta + 1)^2 - 8(v^*\beta - 1) = (\beta + 1 - 4v^*)^2 + 8(1 - v^*)(1 + 2v^*) > 0 \tag{A.4}$$

So Eq. (9) has two different real roots.

**Appendix B**

Here, the stress distribution is given for FG hollow cylinder under three boundary conditions. The detailed process is as follows.

When  $\delta = 0$ , the stress distributions Eqs. (17)–(20) under three different boundary conditions can degenerate to get the stress distribution of the FG thick walled cylinder.

The radial stress and the circumferential stress of the hollow cylinder in Case A are

$$\begin{aligned} \sigma_r &= r^{\beta-1} \left(\frac{a}{R}\right)^{1-\beta} \frac{\left(P + Q\left(\frac{a}{R}\right)^{m_1-1} \left(\frac{a}{R}\right)^\beta\right)r^{m_2} - \left(P + Q\left(\frac{a}{R}\right)^\beta \left(\frac{a}{R}\right)^{m_2-1}\right)r^{m_1}}{\left(\left(\frac{a}{R}\right)^{m_1} - \left(\frac{a}{R}\right)^{m_2}\right)} \\ \sigma_\theta &= \frac{\left(\frac{a}{R}\right)^{1-\beta} r^{\beta-1} (\chi_1 - \chi_2)}{[m_1(v - 1) - v][m_2(v - 1) - v] \left(\left(\frac{a}{R}\right)^{m_1} - \left(\frac{a}{R}\right)^{m_2}\right)} \end{aligned} \tag{B.1}$$

where

$$\begin{cases} m_1 = \frac{1}{2} \left(-\beta - \sqrt{\beta^2 - 4(v^*\beta - 1)}\right) \\ m_2 = \frac{1}{2} \left(-\beta + \sqrt{\beta^2 - 4(v^*\beta - 1)}\right) \\ \chi_1 = \left(P + Q\left(\frac{a}{R}\right)^\beta \left(\frac{a}{R}\right)^{m_1-1}\right)r^{m_2} (vm_2 + 1 - v)(m_1(1 - v) + v) \\ \chi_2 = \left(P + Q\left(\frac{a}{R}\right)^\beta \left(\frac{a}{R}\right)^{m_2-1}\right)r^{m_1} (vm_1 + 1 - v)(m_2(1 - v) + v) \end{cases} \tag{B.2}$$

The radial stress and the circumferential stress of the hollow cylinder in Case B are

$$\begin{aligned} \sigma_r &= \frac{Qr^\beta \left(\left(\frac{a}{R}\right)^{m_1} r^{m_2-1} (m_2(1 - v) + v) - \left(\frac{a}{R}\right)^{m_2} r^{m_1-1} (m_1(1 - v) + v)\right)}{\left(\frac{a}{R}\right)^{m_1} (m_2(1 - v) + v) - \left(\frac{a}{R}\right)^{m_2} (m_1(1 - v) + v)} \\ \sigma_\theta &= \frac{Qr^\beta \left(\left(\frac{a}{R}\right)^{m_1} r^{m_2-1} (1 - v + m_2v) - \left(\frac{a}{R}\right)^{m_2} r^{m_1-1} (m_1v + 1 - v)\right)}{\left(\frac{a}{R}\right)^{m_1} (m_2(1 - v) + v) - \left(\frac{a}{R}\right)^{m_2} (m_1(1 - v) + v)} \end{aligned} \tag{B.3}$$

where the meanings of  $m_1$  and  $m_2$  are consistent with those in Eq. (B.2).

The radial stress and the circumferential stress of the hollow cylinder in Case C are

$$\begin{aligned} \sigma_r &= \frac{Pr^\beta \left((1 - v)(m_2r^{m_2-1} - m_1r^{m_1-1}) + v(r^{m_2-1} - r^{m_1-1})\right)}{\left(\frac{a}{R}\right)^{\beta+m_1-1} (m_1(1 - v) + v) - \left(\frac{a}{R}\right)^{\beta+m_2-1} (m_2(1 - v) + v)} \\ \sigma_\theta &= \frac{Pr^\beta \left((1 - v)(r^{m_2-1} - r^{m_1-1}) + v(m_2r^{m_2-1} - m_1r^{m_1-1})\right)}{\left(\frac{a}{R}\right)^{\beta+m_1-1} (m_1(1 - v) + v) - \left(\frac{a}{R}\right)^{\beta+m_2-1} (m_2(1 - v) + v)} \end{aligned} \tag{B.4}$$

where the meanings of  $m_1$  and  $m_2$  are consistent with those in Eq. (B.2).

### Appendix C

Here, the stress distribution is given for FG spherical shell under three boundary conditions. When  $\delta = 1$ , the stress distributions Eqs. (17)–(20) under three different boundary conditions can degenerate to get the stress distribution of the FG spherical shell.

The radial stress and the circumferential stress of the spherical shell in Case A are

$$\sigma_r = r^{\beta-1} \left(\frac{a}{R}\right)^{1-\beta} \frac{\left(P + Q\left(\frac{a}{R}\right)^{m_1-1} \left(\frac{a}{R}\right)^\beta\right)r^{m_2} - \left(P + Q\left(\frac{a}{R}\right)^\beta \left(\frac{a}{R}\right)^{m_2-1}\right)r^{m_1}}{\left((a/R)^{m_1} - (a/R)^{m_2}\right)} \quad (\text{C.1})$$

$$\sigma_\theta = \frac{(a/R)^{1-\beta} r^{\beta-1} (\chi_1 - \chi_2)}{[m_1(v-1) - 2v][m_2(v-1) - 2v] \left((a/R)^{m_1} - (a/R)^{m_2}\right)}$$

where

$$\begin{cases} m_1 = \frac{1}{2} \left( -\beta - 1 - \sqrt{(\beta+1)^2 - 8(v^*\beta - 1)} \right) \\ m_2 = \frac{1}{2} \left( -\beta - 1 + \sqrt{(\beta+1)^2 - 8(v^*\beta - 1)} \right) \end{cases} \quad (\text{C.2})$$

$$\begin{cases} \chi_1 = \left( P + Q(a/R)^\beta (a/R)^{m_1-1} \right) r^{m_2} (vm_2 + 1) (m_1(1-v) + 2v) \\ \chi_2 = \left( P + Q(a/R)^\beta (a/R)^{m_2-1} \right) r^{m_1} (vm_1 + 1) (m_2(1-v) + 2v) \end{cases}$$

The radial stress and the circumferential stress of the spherical shell in Case B are

$$\sigma_r = \frac{Qr^\beta \left( (a/R)^{m_1} r^{m_2-1} (m_2(1-v) + 2v) - (a/R)^{m_2} r^{m_1-1} (m_1(1-v) + 2v) \right)}{(a/R)^{m_1} (m_2(1-v) + 2v) - (a/R)^{m_2} (m_1(1-v) + 2v)} \quad (\text{C.3})$$

$$\sigma_\theta = \frac{Qr^\beta \left( (a/R)^{m_1} r^{m_2-1} (1 + m_2v) - (a/R)^{m_2} r^{m_1-1} (m_1v + 1) \right)}{(a/R)^{m_1} (m_2(1-v) + 2v) - (a/R)^{m_2} (m_1(1-v) + 2v)}$$

where the meanings of  $m_1$  and  $m_2$  are consistent with those in Eq. (C.2).

The radial stress and the circumferential stress of the spherical shell in Case C are

$$\sigma_r = \frac{Pr^\beta \left( (1-v)(m_2r^{m_2-1} - m_1r^{m_1-1}) + 2v(r^{m_2-1} - r^{m_1-1}) \right)}{\left(\frac{a}{R}\right)^{\beta+m_1-1} (m_1(1-v) + 2v) - \left(\frac{a}{R}\right)^{\beta+m_2-1} (m_2(1-v) + 2v)} \quad (\text{C.4})$$

$$\sigma_\theta = \frac{Pr^\beta \left( (1-v)(r^{m_2-1} - r^{m_1-1}) + v(m_2r^{m_2-1} - m_1r^{m_1-1}) + v(r^{m_2-1} - r^{m_1-1}) \right)}{\left(\frac{a}{R}\right)^{\beta+m_1-1} (m_1(1-v) + 2v) - \left(\frac{a}{R}\right)^{\beta+m_2-1} (m_2(1-v) + 2v)}$$

where the meanings of  $m_1$  and  $m_2$  are consistent with those in Eq. (C.2).

### Appendix D

Here, the expressions for displacement and stress of homogeneous materials hollow cylindrical/spherical shell were given as follows. When the parameter  $\beta$  is 0, FG hollow cylinder/spherical shell degenerates into homogeneous hollow cylinder/spherical shell. The  $u_0, \sigma_r^0$  and  $\sigma_\theta^0$  are displacement, radial and circumferential for homogeneous material under three boundary conditions, respectively. The following expressions are the same as the related expressions in the classic literature [22]

The expressions of  $u_0, \sigma_r^0$  and  $\sigma_\theta^0$  for hollow cylinder in Case A are, respectively,

$$u_0 = \frac{Q(1+v)}{\left((a/R)^{-2} - 1\right)E_0} r^{-1} + \frac{Q(1+v)(1-2v)}{\left(1 - (a/R)^2\right)E_0} r \quad (\text{D.1a})$$

$$\sigma_r^0 = Q \frac{(a/R)^{-1} - (a/R)}{(a/R)^{-1} - (a/R)} \quad (\text{D.1b})$$

$$\sigma_\theta^0 = Q \frac{(a/R)^{-2} + r^{-2}}{(a/R)^{-2} - 1} \quad (\text{D.1c})$$

The expressions of  $u_0$ ,  $\sigma_r^0$  and  $\sigma_\theta^0$  for hollow cylinder in Case B are, respectively,

$$u_0 = -\frac{Q(1+v)(1-2v)}{E_0(a/R)^{-2} + E_0(1-2v)}r^{-1} + \frac{Q(1+v)(1-2v)}{E_0 + E_0(a/R)^2(1-2v)}r \quad (\text{D.2a})$$

$$\sigma_r^0 = Q \frac{(a/R)^{-1}(1+v) - (a/R)r^{-2}(3v-1)}{(a/R)^{-1}(1+v) - (a/R)(3v-1)} \quad (\text{D.2b})$$

$$\sigma_\theta^0 = Q \frac{(a/R)^{-1}(1+v) - (a/R)r^{-2}(1-v)}{(a/R)^{-1}(1+v) - (a/R)(3v-1)} \quad (\text{D.2c})$$

The expressions of  $u_0$ ,  $\sigma_r^0$  and  $\sigma_\theta^0$  for hollow cylinder in Case C are, respectively,

$$u_0 = \frac{P(1+v)(1-2v)}{E_0(a/R)^{-2}(1-2v) + E_0}r^{-1} - \frac{P(1+v)(1-2v)}{E_0(a/R)^{-2}(1-2v) + E_0}r \quad (\text{D.3a})$$

$$\sigma_r^0 = P \frac{(1-v)(1+r^{-2}) + v(1-r^{-2})}{((a/R)^{-2}(2v-1) - 1)} \quad (\text{D.3b})$$

$$\sigma_\theta^0 = P \frac{(1-v)(1-r^{-2}) + v(1+r^{-2})}{((a/R)^{-2}(2v-1) - 1)} \quad (\text{D.3c})$$

The expressions of  $u_0$ ,  $\sigma_r^0$  and  $\sigma_\theta^0$  for spherical shell in Case A are, respectively,

$$u_0 = \frac{Q(1+v)}{2((a/R)^{-3} - 1)E_0}r^{-2} + \frac{Q(1-2v)}{(1 - (a/R)^3)E_0}r \quad (\text{D.4a})$$

$$\sigma_r^0 = Q \frac{(a/R)^{-3} - r^{-3}}{(a/R)^{-3} - 1} \quad (\text{D.4b})$$

$$\sigma_\theta^0 = Q \frac{2(a/R)^{-3} + r^{-3}}{2((a/R)^{-3} - 1)} \quad (\text{D.4c})$$

The expressions of  $u_0$ ,  $\sigma_r^0$  and  $\sigma_\theta^0$  for spherical shell in Case B are, respectively,

$$u_0 = -\frac{Q(1+v)(1-2v)}{(a/R)^{-3}E_0(1+v) + 2E_0(1-2v)}r^{-2} + \frac{Q(1+v)(1-2v)}{E_0(1+v) + 2E_0(a/R)^3(1-2v)}r \quad (\text{D.5a})$$

$$\sigma_r^0 = Q \frac{(a/R)^{-2}(1+v) - (a/R)r^{-3}(4v-2)}{(a/R)^{-2}(1+v) - (a/R)(4v-2)} \quad (\text{D.5b})$$

$$\sigma_\theta^0 = Q \frac{(a/R)^{-2}(1+v) - (a/R)r^{-3}(1-2v)}{(a/R)^{-2}(1+v) - (a/R)(4v-2)} \quad (\text{D.5c})$$

The expressions of  $u_0$ ,  $\sigma_r^0$  and  $\sigma_\theta^0$  spherical shell in Case C are, respectively,

$$u_0 = -\frac{P(1+v)(1-2v)}{2(a/R)^{-3}E_0(2v-1) - E_0(1+v)}r^{-2} + \frac{P(1+v)(1-2v)}{2(a/R)^{-3}E_0(2v-1) - E_0(1+v)}r \quad (\text{D.6a})$$

$$\sigma_r^0 = P \frac{(1-v)(1+2r^{-3}) + 2v(1-r^{-3})}{(a/R)^{-3}(4v-2) - (1+v)} \quad (\text{D.6b})$$

$$\sigma_\theta^0 = P \frac{(1-v)(1-r^{-3}) + v(2+r^{-3})}{(a/R)^{-3}(4v-2) - (1+v)} \quad (\text{D.6c})$$

## Appendix E

Here, the numerical calculation process when the both Young's modulus and Poisson's ratio change with thickness distribution of cylinder/shell in the form of power functions is given. It is assumed that the radially varying Young's modulus and Poisson's ratio are approximated by  $E(r) = E_0 r^\beta$  and  $\nu(r) = \nu_0 r^\alpha$ , respectively.

Constitutive equations are

$$\begin{aligned}\sigma_r &= c_{11}(r)\varepsilon_r + (\delta + 1)c_{12}(r)\varepsilon_\theta \\ \sigma_\theta &= c_{12}(r)\varepsilon_r + c_{11}(r)\varepsilon_\theta + \delta c_{12}(r)\varepsilon_\phi\end{aligned}\quad (\text{E.1})$$

where

$$\begin{aligned}c_{11}(r) &= \frac{E_0(1 - \nu_0 r^\alpha)r^\beta}{(1 + \nu_0 r^\alpha)(1 - 2\nu_0 r^\alpha)} \\ c_{12}(r) &= \frac{E_0\nu_0 r^{\alpha+\beta}}{(1 + \nu_0 r^\alpha)(1 - 2\nu_0 r^\alpha)}\end{aligned}\quad (\text{E.2})$$

Using Eqs. (E.1) and (4), the governing equation for radial displacement can be expressed as

$$u'' + p(r)u' + q(r)u = 0 \quad (\text{E.3})$$

where

$$\begin{aligned}p(r) &= \frac{1}{r} \left( \frac{F_1 r^{2\alpha} + F_2 r^{3\alpha} + F_3 r^\alpha + \beta}{(2\nu_0 r^\alpha - 1)(\nu_0^2 r^{2\alpha} - 1)} + (\delta + 1) \right), \\ q(r) &= \frac{1}{r^2} (\delta + 1) \left[ \frac{\nu_0 r (F_4 r^{3\alpha-1} + F_5 r^{2\alpha-1} + F_6 r^{\alpha-1})}{(2\nu_0 r^\alpha - 1)(\nu_0^2 (r^\alpha)^2 - 1)} - 1 \right], \\ F_1 &= 4 \left( \alpha - \frac{\beta}{4} \right) \nu_0^2, \quad F_2 = -2\nu_0^3 (\alpha - \beta), \quad F_3 = -2\beta\nu_0 \\ F_4 &= 2\nu_0^2 (\alpha - \beta), \quad F_5 = -\beta\nu_0, \quad F_6 = \alpha + \beta\end{aligned}\quad (\text{E.4})$$

Equation (E.3) is a second-order ordinary differential boundary-value problem. The finite difference method is used to solve this problem in this paper.

On the internal node  $r_i$ , one marks as  $u(r_i) = u_i$ ,  $p(r_i) = p_i$  and  $q(r_i) = q_i$ . On each node, replace the first and second derivatives with first and second differences, respectively. The difference expressions of  $u'$  and  $u''$  are approximated

$$u'(r_i) = \frac{du}{dr} = \frac{u_i - u_{i-1}}{h}, \quad u''(r_i) = \frac{d^2u}{dr^2} = \frac{u_{i+1} - 2u_i + u_{i-1}}{h^2} \quad (\text{E.5})$$

where  $a$  and  $R$  are the inner diameter and outer diameter of the cylinder/spherical shell, respectively. The solution interval is divided into  $N$  equal parts, where the points are  $r_0 = a/R$ ,  $r_i = r_0 + ih$ , ( $i = 0, 1, 2 \dots N$ ) and  $h = (R - a)/N$ . Then, Eq. (E.3) is written as

$$\frac{u_{i+1} - 2u_i + u_{i-1}}{h^2} + p_i \frac{u_i - u_{i-1}}{h} + q_i u_i = 0, \quad (i = 1, 2 \dots N - 1) \quad (\text{E.6})$$

At the edge nodes,  $i = 0$  and  $i = N$

$$u'_0 = \frac{u_1 - u_0}{h}, \quad u'_N = \frac{u_N - u_{N-1}}{h} \quad (\text{E.7})$$

For Case A, using Eqs. (E.1) and (E.7), boundary condition can be written as

$$\begin{aligned}i = 0, \quad & \left( \frac{(\delta + 1)c_{12}(r_0)}{a} - \frac{c_{11}(r_0)}{h} \right) u_0 + \frac{c_{11}(r_0)}{h} u_1 = -P \\ i = N, \quad & -\frac{c_{11}(1)}{h} u_{N-1} + \left( \frac{c_{11}(1)}{h} + \frac{(\delta + 1)c_{12}(1)}{1} \right) u_N = Q\end{aligned}\quad (\text{E.8})$$

And Eq. (E.6) can be rewritten as

$$a_i u_{i-1} + b_i u_i + c u_{i+1} = 0, 1 \leq i \leq N - 1 \tag{E.9}$$

where

$$a_i = 1 - p_i h \quad b_i = p_i h + h^2 q_i - 2 \quad c = 1 \tag{E.10}$$

Next, the displacement can be solved numerically. Using Eqs. (E.2)–(E.9), it yields

$$\begin{bmatrix} \frac{(\delta+1)c_{12}(r_0)}{a} - \frac{c_{11}(r_0)}{h} & \frac{c_{11}(r_0)}{h} & 0 & 0 & \dots & 0 \\ a_1 & b_1 & c & 0 & \dots & 0 \\ 0 & a_2 & b_2 & c & \dots & 0 \\ 0 & 0 & a_3 & b_3 & \ddots & \vdots \\ \vdots & \vdots & \vdots & \vdots & b_{N-1} & c \\ 0 & 0 & 0 & 0 & -\frac{c_{11}(1)}{h} & \frac{c_{11}(1)}{h} + \frac{(\delta+1)c_{12}(1)}{R} \end{bmatrix} \begin{bmatrix} u_0 \\ u_1 \\ u_2 \\ \vdots \\ u_{N-1} \\ u_N \end{bmatrix} = \begin{bmatrix} -P \\ 0 \\ 0 \\ \vdots \\ 0 \\ Q \end{bmatrix} \tag{E.11}$$

For Case B, using Eqs. (E.1) and (E.7), boundary condition can be written as

$$\begin{aligned} i = 0, \quad u_0 = 0 \\ i = N, \quad -\frac{c_{11}(1)}{h} u_{N-1} + \left( \frac{c_{11}(1)}{h} + \frac{(\delta+1)c_{12}(1)}{R} \right) u_N = Q \end{aligned} \tag{E.12}$$

Equation (E.11) can be written as

$$\begin{bmatrix} 1 & 0 & 0 & 0 & \dots & 0 \\ a_1 & b_1 & c & 0 & \dots & 0 \\ 0 & a_2 & b_2 & c & \dots & 0 \\ 0 & 0 & a_3 & b_3 & \ddots & \vdots \\ \vdots & \vdots & \vdots & \vdots & b_{N-1} & c \\ 0 & 0 & 0 & 0 & -\frac{c_{11}(1)}{h} & \frac{c_{11}(1)}{h} + \frac{(\delta+1)c_{12}(1)}{R} \end{bmatrix} \begin{bmatrix} u_0 \\ u_1 \\ u_2 \\ \vdots \\ u_{N-1} \\ u_N \end{bmatrix} = \begin{bmatrix} 0 \\ 0 \\ 0 \\ \vdots \\ 0 \\ Q \end{bmatrix} \tag{E.13}$$

For Case C, using Eq. (E.1) and (E.7), boundary condition can be written as

$$\begin{aligned} i = 0, \quad \left( \frac{(\delta+1)c_{12}(r_0)}{a} - \frac{c_{11}(r_0)}{h} \right) u_0 + \frac{c_{11}(r_0)}{h} u_1 = -P \\ i = N, \quad u_N = 0 \end{aligned} \tag{E.14}$$

Equation (E.11) can be written as

$$\begin{bmatrix} \frac{(\delta+1)c_{12}(r_0)}{a} - \frac{c_{11}(r_0)}{h} & \frac{c_{11}(r_0)}{h} & 0 & 0 & \dots & 0 \\ a_1 & b_1 & c & 0 & \dots & 0 \\ 0 & a_2 & b_2 & c & \dots & 0 \\ 0 & 0 & a_3 & b_3 & \ddots & \vdots \\ \vdots & \vdots & \vdots & \vdots & b_{N-1} & c \\ 0 & 0 & 0 & 0 & 0 & 1 \end{bmatrix} \begin{bmatrix} u_0 \\ u_1 \\ u_2 \\ \vdots \\ u_{N-1} \\ u_N \end{bmatrix} = \begin{bmatrix} -P \\ 0 \\ 0 \\ \vdots \\ 0 \\ 0 \end{bmatrix} \tag{E.15}$$

Next, the displacement can be solved numerically. The radial stress and circumferential stress are obtained by substituting Eqs. (E.2), (E.5), (E.7) and Eq. (1) into Eq. (E1).

## References

1. Tutuncu, N., Ozturk, M.: Exact solutions for stresses in functionally graded pressure vessels. *Compos. B* **32**, 483–486 (2001)
2. Niino, M., Hirai, T., Watanabe, R.: The functionally gradient materials. *Jpn J. Appl. Phys.* **13**, 257–264 (1984)
3. Zhong, Z., Yu, T.: Analytical solution of a cantilever functionally graded beam. *Compos. Sci. Technol.* **67**, 481–488 (2007)
4. Li, X.F.: A unified approach for analyzing static and dynamic behaviors of functionally graded Timoshenko and Euler-Bernoulli beams. *J. Sound Vib.* **318**, 1210–1229 (2008)
5. Chu, L.L., Dui, G.S.: Exact solutions for functionally graded micro-cylinders in first gradient elasticity. *Int. J. Mech. Sci.* **148**, 366–373 (2018)
6. Pradhan, K.K., Chakraverty, S.: Free vibration of Euler and Timoshenko functionally graded beams by Rayleigh-Ritz method. *Compos. B* **51**, 175–184 (2013)
7. Kang, Y.A., Li, X.F.: Large deflections of a non-linear cantilever functionally graded beam. *J REINF PLAST COMP.* **29**, 1761–1774 (2010)
8. Li, X.F.: A higher-order theory for static and dynamic analyses of functionally graded beams. *Arch. Appl. Mech.* **80**, 1197–1212 (2010)
9. Jiang, A.M., Ding, H.J.: The analytical solutions for orthotropic beam (II): Solutions for density functionally graded beams. *J. Zhejiang Univ-SC B.* **6**, 155–158 (2005)
10. Ding, H.J., Huang, D.J., Chen, W.Q.: Elasticity solutions for plane anisotropic functionally graded beams. *Int. J. Solids St.* **44**, 176–196 (2007)
11. Horgan, C.O., Chan, A.M.: The pressurized hollow cylinder or disk problem for functionally graded isotropic linearly elastic materials. *J. Elast.* **55**, 43–59 (1999)
12. Sarathchandra, D.T., Kanmani, S.S., Venkaiah, N.: Modeling and analysis of functionally graded cylindrical shell. *Mater. Today.* **5**, 8587–8595 (2018)
13. Horgan, C.O., Chan, A.M.: The stress response of functionally graded isotropic linearly elastic rotating disks. *J. Elast.* **55**, 219–230 (1999)
14. Li, X.Y., Ding, H.J., Chen, W.Q.: Axisymmetric elasticity solutions for a uniformly loaded annular plate of transversely isotropic functionally graded materials. *Acta Mech.* **196**, 139–159 (2008)
15. Tutuncu, N., Temel, B.: A novel approach to stress analysis of pressurized FGM cylinders, disks and spheres. *Compos Struct.* **91**, 385–390 (2009)
16. Ghannad, M., Rahimi, G.H., Zamani, N.M.: Elastic analysis of pressurized thick cylindrical shells with variable thickness made of functionally graded materials. *Compos. B* **45**, 388–396 (2013)
17. Li, X.F., Peng, X.L., Kang, Y.A.: Pressurized hollow spherical vessels with arbitrary radial nonhomogeneity. *AIAA J.* **47**, 2262–2265 (2009)
18. Chirag, S., Srikant, S.P.: Functionally graded cylinders: asymptotically exact analytical formulations. *Appl. Math. Model.* **54**, 782–802 (2018)
19. Bahtui, A., Eslami, M.R.: Coupled thermoelasticity of functionally graded cylindrical shells. *Mech. Res. Commun.* **34**, 1–18 (2007)
20. Bahtui, A., Eslami, M.R.: Generalized coupled thermoelasticity of functionally graded cylindrical shells. *Int. J. Numer. Meth. Eng.* **69**, 676–697 (2007)
21. Jabbari, M., Bahtui, A., Eslami, M.R.: Axisymmetric mechanical and thermal stresses in thick short length FGM cylinders. *Int. J. Pres. Ves. Pip.* **86**, 296–306 (2009)
22. Love, A.E.H.: A treatise on the mathematical theory of elasticity. Cambridge University Press, Cambridge (1892)
23. Shi, P.P., Xie, J.: Revisiting classic problems of exact solutions for stresses in functionally graded pressure vessels. *Mech. Res. Commun.* **20**, 103609 (2020)
24. Shi, P.P., Xie, J., Hao, S.: Static response of functionally graded piezoelectric-piezomagnetic hollow cylinder/spherical shells with axial/spherical symmetry. *J Mech Sci Technol.* **35**, 1518–1532 (2021)